Dynamic Structure Factor of Diblock Copolymer Solutions in the Disordered State. 1. Far from the Ordering Transition

R. Sigel,[†] S. Pispas,[‡] N. Hadjichristidis,[†,‡] D. Vlassopoulos,[†] and G. Fytas*[,†]

Institute of Electronic Structure and Laser, Foundation for Research and Technology−Hellas (FORTH), 71110 Heraklion, Crete, Greece, and Department of Chemistry, University of Athens, 15771 Athens, Greece

Received July 22, 1999

ABSTRACT: The dynamic structure factor of entangled solutions of very high molecular weight styrene−isoprene (SI) diblock copolymers in the common solvent toluene is studied by photon correlation spectroscopy. The intermediate scattering function $S(q,t)$ with wave vector **q** spanning the peak position q^* of the static structure factor $S(q)$ displays three relaxation processes in the homogeneous disordered state far away from the order-to-disorder (ODT) transition. In this regime, the systems investigated are marginally entangled. To examine the sensitivity of the shape of $S(q,t)$ with regard to polydispersity and composition we report experimental $S(q,t)$ of one symmetric and two asymmetric SI with different distributions. In all cases, chain self-diffusion and two chain conformational motions describe the experimental $S(q,t)$. The main contribution to $S(q \approx q^*,t)$ originates from the slow (reptation-like) chain motion with rate $\Gamma_1 = O(\tau_1^{-1})$ where the longest relaxation time τ_1 is obtained by dynamic mechanical shear measurements. The unexpected findings relate to the stronger contribution of fast (Rouse-like) to the $S(q \approx q^*,t)$ of the asymmetric SI rich in I ($f_s = 0.26$) and the increase of the $S(q \simeq 0)$ due to polydispersity with concentration in the homogeneous state.

I. Introduction

The dynamic structure factor, $S(q,t) = \langle \psi_{\mathbf{q}}(t)\psi_{-\mathbf{q}}(0)\rangle$, with $\psi_{\mathbf{q}}$ being the order parameter (composition) fluctuation of wave vector **q**, of ideally monodisperse diblock copolymers (BC) can be represented by a single-exponential decay function:[1]

$$S(q,t) = S(q)\exp[-\Gamma_1(q)t], \quad \Gamma_1(q) = xg(1,x)/(\tau_1 S(q)) \tag{1}$$

The static structure factor $S(q)$ attains its maximum at finite $x^* = (q^*R)^2$ ($\simeq$4 for symmetric BC) while at low x ($<$1), $S(q) \propto x$; R being the radius of gyration. These long wavelength fluctuations $\psi_{\mathbf{q}}(t)$ relax with a characteristic time, (Γ_1^{-1}), on the order of the chain longest relaxation time, i.e., $\Gamma_1 \approx 1/\tau_1$ in accordance to the mean field prediction of eq 1; for $x < 1$, the chain form factor, $g(1,x) \simeq 1$.

Au: Our style uses italics for variables. Please note that subscripts to variables are only made italic if they, too, are variables. Vectors and tensors are boldface roman in our style, though magnitudes of vectors and tensors are considered to be variables and thus are made italic. Please verify our usage, especially with q, which apparently can represent a vector in some cases but a variable in others.

This low x fraction of $S(q,t)$ has been reported for BC melts[2] and semidilute solutions[3] in neutral solvent using photon correlation spectroscopy (PCS). However, these earlier works have revealed the presence of a second dynamic contribution in $S(q < q^*,t)$ with characteristic q-independent intensity S_2 and diffusive rate Γ_2 yielding the self-diffusion D_s:

$$S_2 = \kappa_0 q^0/[1 - 2\chi N\kappa_0\phi^{1.6}], \quad \Gamma_2 = D_s q^2[1 - 2\chi N\kappa_0\phi^{1.6}] \tag{2}$$

This process has been identified[3] as the chain self-diffusion detected due to the finite composition polydispersity κ_0 and the refractive index contrast between the two blocks. Hence, the excess S_2 arises from extra composition fluctuations due to polydispersity. Further, enhancement of the composition polydispersity in the low x range[4] is accommodated in this process (eq 2) whereas the mean field contribution eq 1 remains essentially unchanged irrespectively to the proximity to the ODT. However, for higher molecular weight (M_w) BC with access to larger x, the thermodynamic interactions become important, and the relative contribution of $S(q)$ and the excess S_2 can significantly change, affecting the shape of the total $S(q,t)$. In addition, one should bear in mind that the synthesis of high M_w block copolymers by anionic polymerization is bound to exhibit some contamination with homopolymer, and hence fractionation is required. Previous data[5] on a symmetric styrene−isoprene (SI) diblock with $M_w = 1.1 \times 10^6$ show a domination of the chain relaxation (eq 1) whereas for SI with $M_w = 2 \times 10^6$ and 3×10^6 the presence of the diffusive process (eq 2) is overwhelming at $x < x^*$. The ratio $\Gamma_1/\Gamma_2 \approx O(x^{-1})$, so that the two processes can be dynamically resolved[4] for $x < 0.4$ as observed for diblock copolymers with $M_w < 2 \times 10^5$.

In this paper, we address the shape of $S(q,t)$ covering the q range to q^* far from ODT and examine its sensitivity to the block composition and the extent of fractionation.

II. Experimental Section

Polymer Synthesis. The high molecular weight SI diblocks were synthesized by anionic polymerization techniques, which ensure control of molecular weight and narrow polydispersity of the produced polymers. Since the synthesis of high molecular weight block copolymers requires maximum purity of the polymerization mixture, all reagents (solvent, monomers, and terminating agent) were purified by taking special precautions in order to reduce impurities to the minimum possible level. Monomers were collected in *n*-BuLi or dibutylmagnesium

[†] Foundation for Research and Technology−Hellas (FORTH).
[‡] University of Athens.

10.1021/ma991213f CCC: $18.00
Published on Web 11/24/1999

Table 1. Molecular Characteristics of High Molecular Weight Asymmetric Diblocks

sample	$M_w \times 10^{-6}$ (LALLS[a])	$M_{w\,PS} \times 10^{-5}$ (LALLS[a])	wt % PS (NMR[b])	M_w/M_n (SEC[c])
SI2M20	1.93	4.88	26	1.09
SI2M80	1.60	1.34	85	1.15

[a] THF at 25 °C. [b] $CDCl_3$ at 30 °C. [c] THF at 40 °C.

prewashed ampules. Reactions were carried out in all-glass, vacuum sealed reactors, washed with *n*-Buli and rinsed with benzene. *sec*-BuLi, prepared by reaction of *sec*-butyl chloride with excess Li, was used as initiator. Styrene was polymerized first in benzene followed by the polymerization of isoprene. The polymer concentration was always kept below 4% w/v in order to avoid complications from high solution viscosity. Active chains were deactivated by thoroughly degassed methanol. Samples of the first block were isolated by heat sealing the appropriate constrictions. Because of the low concentration of the living ends, some deactivation of the PS block occurred by the addition of isoprene. Solvent/nonsolvent fractionation (toluene/methanol) was employed for the isolation of pure diblocks.

Intermediate and final products were checked by size-exclusion-chromatography (SEC). A Waters system composed of a Waters 600 Pump Controller, a set of four Styragel columns (2 × HR-5E continuous porosity, MW range 10^3-10^7; 1 × HT6, MW range 10^5-10^7; 1 × HMW7 MW, range 10^6-10^7), a Waters 410 differential refractometer, and a Waters 996 photodiode array UV detector interfaced with a computer and calibrated with polystyrene standards was used. Weight-average molecular weights of the PS blocks and the purified diblocks in THF were measured with a Chromatix KMX-6 low angle laser light scattering photometer, operating at $\lambda = 633$ nm. The required d*n*/d*c* values were obtained at the same wavelength with a Chromatix KMX-16 laser differential refractometer. The average composition of the samples was determined by ^{1}H NMR spectroscopy. The molecular characteristics of the samples are given in Table 1.

The SEC traces of the SI2M20 and SI2M80 after two and five fractionations are given in Figure 1a (UV detector). The molecular weight distribution for the SI2M20 sample remains almost unchanged by the degree of fractionation, since the low molecular weight PS block can be efficiently separated from the diblock even after two fractionations. On the other hand, the situation for the SI2M80 is obviously improved in the course of fractionation as shown in Figure 1b. After two fractionations, a considerable amount of PS block remains, since now it is more difficult to separate a 1.6 million diblock from a 1.34 million PS. After five fractionations, the PS impurity has been eliminated, resulting in a narrow distributed SI diblock (Figure 1b).

Photon Correlation Spectroscopy (PCS). The intermediate scattering function $C(q,t) = [(G(q,t) - 1)/f^*]^{1/2}$ is obtained from the experimental intensity autocorrelation function $G(q,t)$ (f^* is the instrumental coherence factor) measured by photon correlation spectroscopy in the polarized geometry under homodyne conditions over a broad time range ($10^{-7}-10^2$ s) at a scattering wave vector $\mathbf{q} = 4\pi n/\lambda(\sin(\theta/2)$ (λ is the laser wavelength in a vacuum, n is the refractive index, and θ is the scattering angle) ranging from 3×10^{-3} to 3.5×10^{-2} nm^{-1}. An ALV-5000 full digital correlator was employed in conjunction with a Nd:YAG laser at $\lambda = 532$ nm.[5] All measurements were carried out at 20 °C. The peak of $S(q) = AR_{VV}(q)/(M_wC)$, with $R_{VV}(q)$ being the Rayleigh ratio, $A \int \equiv N_L\lambda^4/(4\pi^2n^2(dn/dc)^2)$, and N_L being the Avogadro number, for these samples falls within the light-scattering q's as shown in Figure 2 for solutions of SI2M20 and SI2M80 in toluene with volume fraction $\phi \ll \phi_{ODT}$, the volume fraction at which the semidilute solution microphase separates. At these concentrations the contribution of the total polymer concentration fluctuations to the R_{VV} is still important as indicated by the different R_{VV} values in the two solutions at low q's; the contrast to the solvent (d*n*/d*c*) is higher for the SI2M80 solution. Nevertheless,

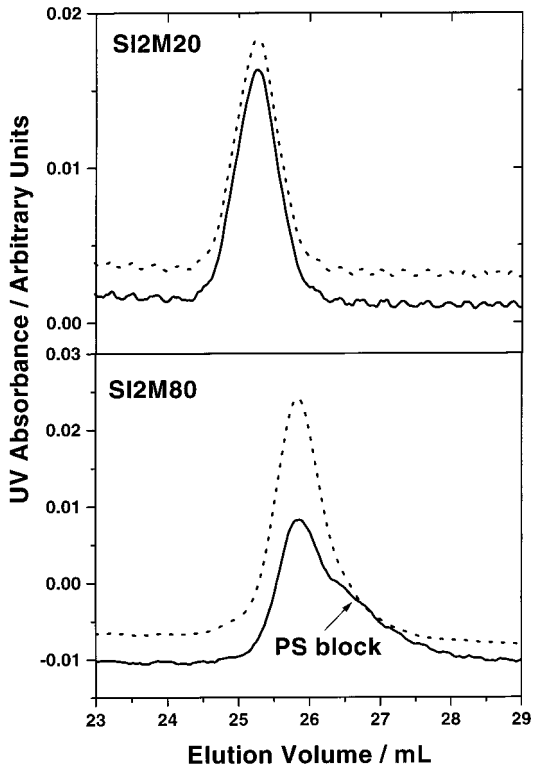

Figure 1. SEC traces (with UV detector) for SI2M20 (a) and SI2M80 (b) obtained after two (solid lines) and five (dotted lines) fractionations of the original samples.

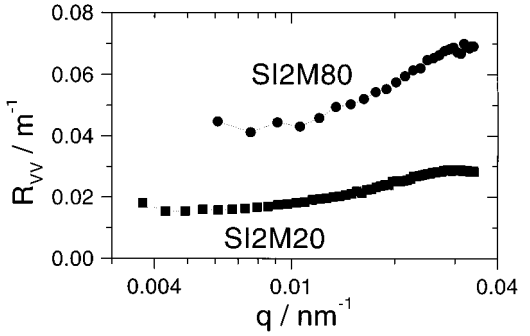

Figure 2. Rayleigh ratio $R_{VV}(q)$ of two solutions of five times fractionated SI2M20 and SI2M80 in toluene at concentrations of 2.2 wt % (●) and 3.9 wt % (■), respectively.

the peak occurs at q^* conforming to the mean field prediction $R^{-1}(\mathbf{f}(1 - f)/3)^{-1/4}$.

Shear Rheology. Complementary dynamic shear mechanical measurements were carried out at 20 °C using a Rheometric Scientific ARES 100FRTN1-HR rheometer in the cone-and-plate geometry (0.04 rad cone angle, 25 mm diameter). Dynamic frequency sweeps were performed in the frequency range 10−500 rad/s within the linear viscoelastic regime.

III. Results and Discussion

1. Dynamics of the Thermal Composition Fluctuations. The intermediate scattering function $C(q,t)$ for 3.9 wt % SI2M80 solution at two values of $q = 3.4 \times 10^{-2}$ nm^{-1} (around q^*) and 9.1×10^{-3} nm^{-1} is shown in Figure 3. The representation of $C(q,t)$ proceeds via inverse Laplace transformation

$$C(q,t) = \int L(\ln \tau) \exp(-t/\tau)\, d(\ln \tau) \qquad (3)$$

the distribution of relaxation times $L(\ln \tau)$ being also included in Figure 3. Three relaxation processes were

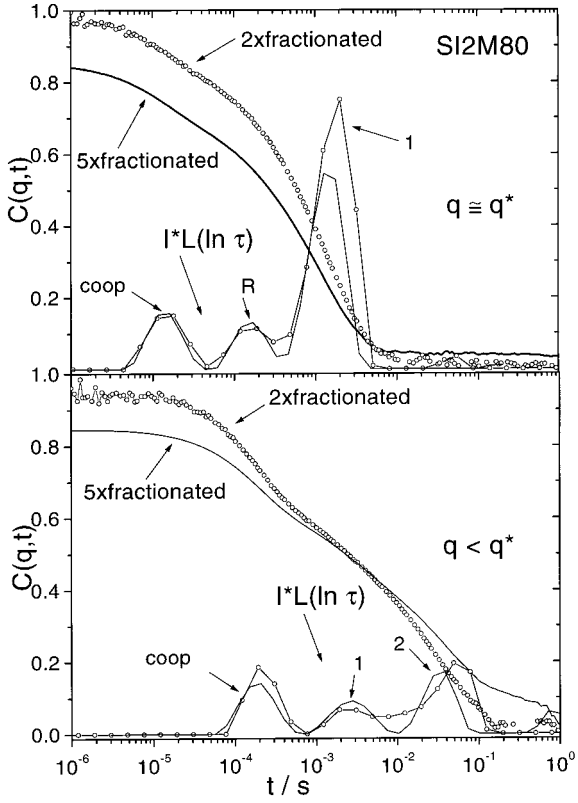

Figure 3. Intermediate scattering functions $C(q,t)$ at q = 0.034 and 9.1×10^{-3} nm^{-1} for 3.9 wt % five times fractionated SI2M80 in toluene at 25 °C along with the normalized distribution of relaxation times $IL(\ln \tau)$ (eq 3). For comparison, the $C(q,t)$ values for SI2M80* (4.3 wt %) obtained after two fractionations are also shown. The peaks of $L(\ln \tau)$ are assigned to the cooperative (coop), self-diffusion (2), and the two chain conformational motions (1 for the reptation and R for the Rouse mode).

found to be the optimum solution of eq 3 based not only on the fit quality but also on the consistent and physically meaningful results. The first peak of $L(\ln \tau)$ at short times relates to the cooperative diffusion responsible for the relaxation of the total polymer concentration fluctuations. The location of the peak, $\tau_c \sim q^{-2}$ and the intensity $I_c = I(q)\alpha_c \sim q^0$ ($I(q)$ is the total scattering intensity and α_c the amplitude of this process) clearly support this assignment. Further, I_c and D_c ($=(\tau_c q^2)^{-1}$) decrease and increase, respectively, with concentration as in the case of semidilute solutions of linear homopolymers.[7] Both D_c and I_c assume very similar values in the two SI2M80 moieties when compared at the same concentration. The decay of the thermal concentration fluctuations driven by the solution osmotic pressure is the fastest process at not very low q's (Figure 3a,b).

The other two slower processes relate to the composition fluctuation $\psi_{\mathbf{q}}(t)$. The third peak of $L(\ln \tau)$ at long times and $q = 9.1 \times 10^{-3}$ nm^{-1} (Figure 3b) exhibits the features of eq 2 with respect to the q dependence for the intensity I_2 ($\propto S_2$) and the time (location of the peak) τ_2 ($=1/\Gamma_2$), and it is the concentration dependence[3] of I_2 and $D_s = (\tau_2 q^2)^{-1}$ that distinguishes this process from the cooperative diffusion; I_2 and D_s, respectively, increase and decrease with concentration. Hence, this process relates to composition fluctuations due to composition polydispersity. However, the third peak at the high $q = 0.034$ nm^{-1} in Figure 3 cannot be identified with the polydispersity (self-diffusion) process based on its q-dependent intensity (see Figure 5 below). Instead, this process at the highest q is identified with the intermediate peak at $q = 9.1 \times 10^{-3}$ nm^{-1}, and relates to the order parameter fluctuations of a monodisperse diblock copolymer (eq 1). At high q's, the intermediate peak of $L(\ln \tau)$ in Figure 3a has the features of curvilinear Rouse-like motion of entangled chains.[5]

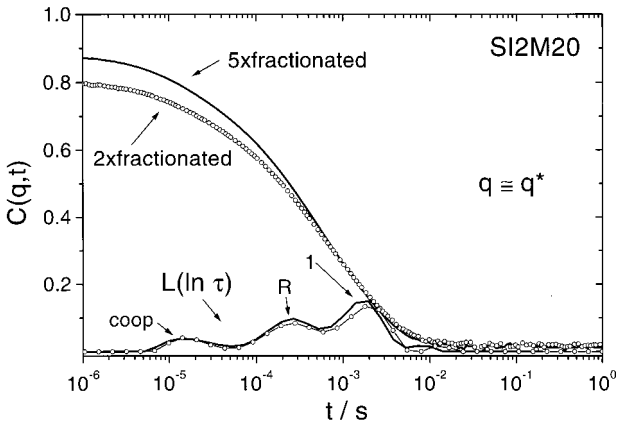

Figure 4. Intermediate scattering functions $C(q,t)$ at q = 0.034 nm^{-1} and 25 °C for 2.2 wt % SI2M-20 after two and five fractionations along with the distribution $L(\ln \tau)$. The notation of the peaks of $L(\ln \tau)$ is that of Figure 3.

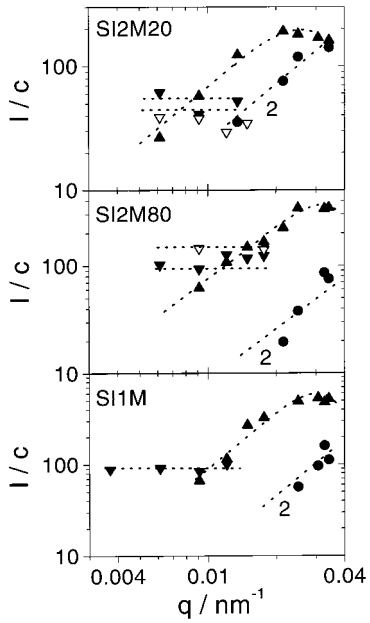

Figure 5. Intensities associated with the composition fluctuations of different wave vectors **q** in the three SI/toluene solutions with concentrations: 2.2 wt % for SI2M20, 3.9% for SI2M80 and 2.5 wt % for SI1M. The empty symbols are for the two fractionations shown for comparison [(▲, ●) chain relaxations; (▼) chain self-diffusion]. The slope 2 is to indicate the q^2 dependence of the intensities I_R and I_1 for the chain relaxations, and the dashed lines are to guide the eye.

Prior to the discussion of the characteristics (intensity and rate) of these processes (section III.2) we will examine the shape sensitivity of $C(q,t)$ with regard to polydispersity and block composition by considering a second SI2M80* (two fractionations) and a SI2M20 with almost mirror composition. The three-peak structure of $L(\ln \tau)$ persists in SI2M80* as shown in Figure 3 for a 4.3 wt % solution. Given the different SEC trace of the SI2M80 (Figure 1b), which is contaminated with some PS homopolymer, this finding is rather unexpected even in the homogeneous mean field regime; SI2M80* should

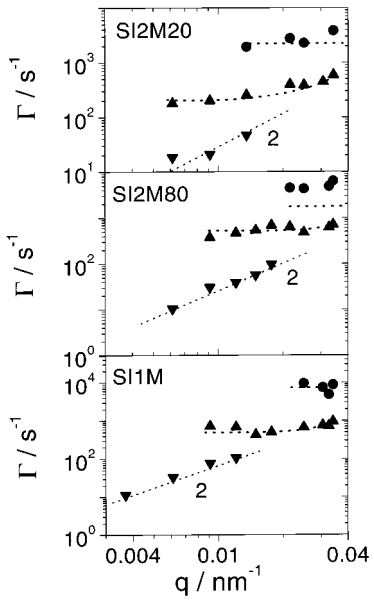

Figure 6. Relaxation rates for the processes of the dynamic structure factor at different q's for the homogeneous SI/toluene solutions. Concentrations and symbols are those used in Figure 5.

exhibit a strong polydispersity process due to the large κ_0. A possible account of it is given in the next section; these two (SI2M80) samples do however have different ϕ_{ODT} values (0.082 and 0.1, respectively, for SI2M80* and SI2M80). For SI2M20, rich in polyisoprene, the only apparent difference is the weaker contribution of the cooperative process (smaller dn/dc than in SI2M80) in the $L(\ln \tau)$, as shown in Figure 4 for two fractions of SI2M20 at 2.2 wt %. The similar $C(q,t)$ in the homogeneous state for these two SI2M20 fractions is in accord with their SEC traces (Figure 1a), which further justifies the close values for ϕ_{ODT} (7.3 and 7.4 wt % respectively for SI2M20* and SI2M20).

2. Analysis of the Processes. Figures 5 and 6 show the intensities I_i/c and relaxation rates Γ_i associated with $\psi_{\mathbf{q}}$ relaxing via self-diffusion and chain motions in the three samples. The cooperative diffusion is found to exhibit the expected behavior for the semidilute solutions of homopolymer providing a strong support of the data analysis; it is therefore not shown here.

The polydispersity process at $q < 0.01$ nm^{-1} conforms to eq 2, displaying a diffusive rate Γ_2 and virtually q-independent intensity I_2. In the vicinity of the most probable $\psi_{\mathbf{q}}$ with $q \simeq q^*$, $\psi_{\mathbf{q}}(t)$ relaxes by a q-independent rate Γ_1 and the associated intensity I_1 expectedly increases with q. In this q range ($q > 0.01$ nm^{-1}), the polydispersity process can be hardly resolved since $\Gamma_2(q) \simeq O(\Gamma_1)$ and $I_2 < I_1(q)$. Instead, the additional process evolved between cooperative and main relaxation (Figures 3a, 4) with $\Gamma_R \sim q^0$ and $I_R \sim q^2$ is responsible for the relaxation of $\psi_{\mathbf{q}}(t)$ of the entangled (see below) SI solutions at short times ($\Gamma_1 t \ll 1$). In the reptation model,[7] this fast process can be assigned[5] to tube length fluctuations modeled by curvilinear Rouse-like motion whereas tube conformational fluctuations via chain reptation can be associated with the slower rate Γ_1. All five samples unambiguously exhibit unique dynamic behavior for the order parameter fluctuations in the disordered state.

Concerning the composition polydispersity process, SI2M80* has a slightly higher I_2 than SI2M80 (Figure 5) despite the different SEC traces (Figure 1b). Envisaging SI2M80* as a mixture of PS homopolymer ($f_s = 1$) with volume fraction ϕ_s and degree of polymerization N_1 (=13900) and SI ($f_s = 0.85$) with $\tilde{\phi}_s \equiv 1 - \phi_s$ and $N_2 = 17640$, the composition polydispersity parameter $\kappa_0 = \langle f_s^2 \rangle - \langle f_s \rangle^2$, can be estimated by $\kappa_0 = (\phi_s + \tilde{\phi}_s f_s^2) - (\phi_s N_1 + \tilde{\phi}_s N_2 f_s)/(\phi_s N_1 + \tilde{\phi}_s N_2)^2$. Its value is actually comparable to the inherent[3]

$$\kappa_0 \simeq 2(M_w/M_n - 1) f_s^2 (1 - f_s^2)/[f_s^2 + (1 - f_s)^2] \quad (3a)$$

obtained for independent molecular weight distributions of S and I blocks in SI2M80 if the PS fraction is small i.e., $f_s \simeq 0.1$.

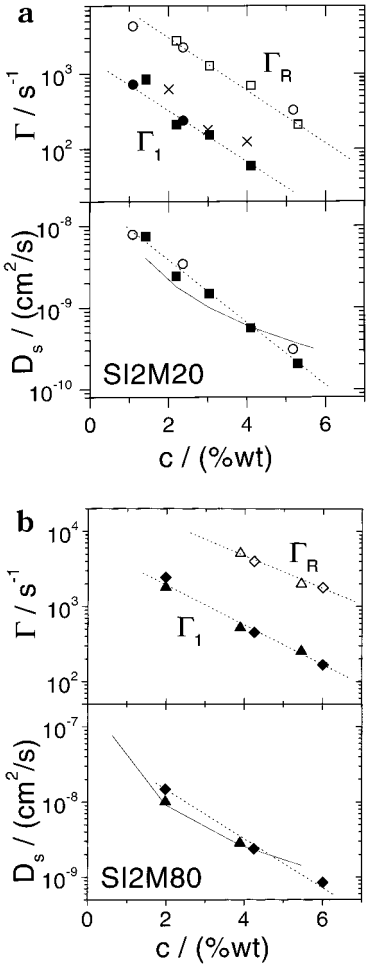

Figure 7. Chain self-diffusion (D_s) and relaxation rates (Γ_1, Γ_R) of SI2M20 (a) and SI2M80 (b) at different concentrations in the homogeneous mean field regime. Γ_R: ○, □. Γ_1: ●, ■. D_s: ●, ■. Symbols are for two (circles) and five (squares) fractionations and × (in a) the relaxation rate $1/\tau_1$ from the dynamic shear measurements (two times fractionated SI2M20). The dashed lines are to guide they eye whereas the solid lines denote the scaling dependence $D_s \sim c^{-1.8}$ for entangled polymer solutions.

Figure 7 shows the concentration dependence of the diffusion coefficient D and the two relaxation rates Γ_1 and Γ_R of the order parameter fluctuations (for a nominally monodisperse diblock) in the two asymmetric SI's. All three dynamic quantities display similar rate of decrease with concentration. The conformity of the q and c dependence of the three processes to the predicted dynamics of $S(q,t)$ of homogeneous entangled diblock solutions is discussed in the next section.

3. Relaxation Mechanisms. The slow diffusive process of $C(q,t)$ supports the two predictions of eq 2

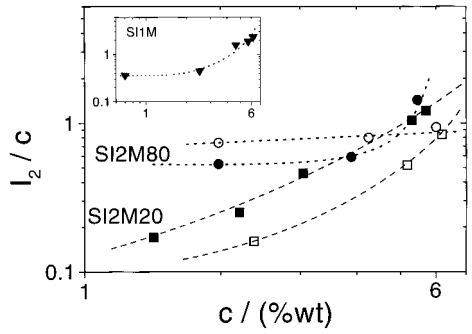

Figure 8. Reduced intensity I_2/c associated with the diffusive polydispersity process in the three SI's (open and solid symbols respectively for the two asymmetric SI after two and five fractionations) at different concentrations.

and can be therefore assigned to SI chain diffusion. In fact, pulsed field gradient (PFG) NMR self-diffusion data on the same samples[8] confirm this assignment. In the entangled regime, ignoring the concentration dependence of the local friction, the predicted[3a] $D_s \sim \phi^{-1.8}$ approximates well the experimental slowing down with concentration $c = \phi\rho$ (ρ being the SI density) (Figure 7) indicating an absence of thermodynamic effects in the homogeneous state. However, the reduced I_2/c for SI2M20 and SI1M, which should be virtually insensitive to concentration variation for typical values of κ_0 (between 0.006 and 0.01) increases strongly with c as visualized in Figure 8; only the SI2M80* which is characterized by a broader SEC trace among the other samples exhibits the c dependence anticipated from eq 2. The extra c dependence of I_2 indicates the presence of interactions other than those encountered in both eqs 2. An attempt to accommodate the $I(c)/c$ changes by eq 2, using unrealistically large κ_0 would have led to much stronger $D(c)$ dependence than that observed experimentally, and deviations from the PFG NMR self-diffusion.[8] The limiting values of I_2/c at low c assume different values among the investigated diblocks. For very similar N and f_s, I_2/c of SI2M80* is almost 40% higher than in SI2M80 as discussed in the preceding section. Between the SI2M20 and SI2M80 the polydispersity κ_0 ($\propto I_2/cN$) of the former is more than three times lower, a trend in semiquantitative agreement with eq 3 and the M_w/M_n values of Table 1. Conversely, the experimental I_2/cN values are a more reliable index of the composition heterogeneities in real BC's.

With regard to the extent of the thermodynamic interactions, all of the present samples are in the homogeneous mean field regime. On the other hand, the classification with respect to the topological constraints is based on the following information: Figure 9 shows typical dynamic shear moduli G' and G'' for SI2M20* at 2 and 5 wt % from which the time $\tau_1 = \omega_1^{-1}$ (upper inset) is extracted by the extrapolation of the low-frequency moduli data $G' \sim \omega^2$ and $G'' \sim \omega$ to the point of intersection. Whereas the terminal flow region has been clearly reached in both solutions, the crossover of moduli at higher frequencies constitutes unambiguous evidence of the presence of entanglements; even for the more dilute 2% solution, the deviation of the high frequency data from the terminal slopes suggests a moduli crossover at frequencies higher than reached experimentally at the temperature of 20 °C. In view of the lack of appropriate theory for diblock copolymers, using the concept of reptation for homopolymers[7b] we can estimate $N/N_e = O(1)$ for the displayed concentrations (Figure 9); N_e is the characteristic number of segments between entanglements. Alternatively, based on the weight-average $N_e^{-1} = [f_S N_{e,S}^{-1/2} + (1 - f_S)N_{e,I}^{-1/2}]^2$, with $N_{e,S} = 150$ and $N_{e,I} = 69$, the values for undiluted PS and PI respectively, and $N_e(\phi) = N_e\phi^{-1.3}$, we can estimate the entanglement volume fractions ϕ_e for SI2M20 and SI2M80 as 0.013 and 0.022, respectively. In accord with these numbers, the SI2M80 at 1.98% shows one process (besides cooperative and polydispersity modes), whereas above 3.9% we have an additional virtually q-independent process as shown in Figure 5. Likewise, for the SI2M20 above 2.2% (also Figure 5), we observe two virtually q-independent processes. Further support comes from the already mentioned concentration dependence of D_s (Figure 7). We therefore classify the present systems as marginally entangled. This means that because of the lack of theory for the Rouse or crossover regimes, we next rationalize the chain dynamics in the framework of the reptation theory.

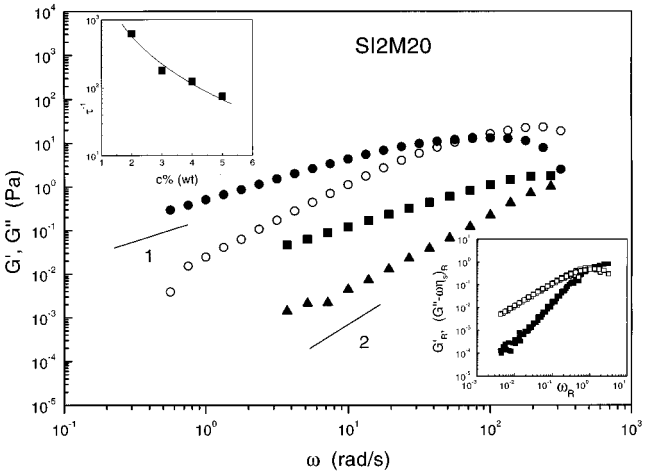

Figure 9. Loss and storage shear modulus for 2% (△) and 5% (○) SI2M20 solutions in toluene at 20 °C. The relaxation rate (inset) obtained from the intersection of G' and G'' is used in the reduced plot in the lower inset ($\omega_R \equiv \omega\tau_1$).

The two intermediate processes between the fast cooperative and slow self-diffusion exhibit q-dependent I_i and q-independent rate $\tilde{A}_i$ characteristic for chain relaxation modes. For $x < x^*$ the dynamic structure factor for pure reptation[5]

$$S(q,t) \simeq (4xf^2(1 - f^2)/\pi^4) \sum_{k=0} (2k + 1)^{-4} \exp[-\pi^2(2k + 1)^2 t/4\tau_1] \quad (4)$$

is insensitive to the thermodynamic interactions and the main relaxation mode ($k = 0$) is characterized by the concentration independent $S(x) = 4f^2(1 - f^2)x/\pi^4$ and q-independent rate $\Gamma_1 = \pi^2/(4\tau_1)$ i.e., the rate Γ_1 (eq 1) should be comparable to the rate τ_1^{-1} obtained from shear rheometry (Figure 9). As expected[2b] for the homogeneous state in the absence of strong fluctuations, G' and G'' can be nicely superimposed to master curves as shown in the lower inset of Figure 9. The light-scattering Γ_1 and mechanical ω_1 compare satisfactorily as indicated by the plot of Figure 7a. In the case of entangled polymer solutions,[5] $\tau_1 \simeq \tau_0(N^3/N_e(\phi))\,\phi^{(2-3\nu)/(3\nu-1)} \propto \phi^{1.6}$. This dependence is not far from the experimental variation (about $\sim c^{-2.0}$) of Figure 7 (dashed line).

The intensity I_1/cN ($\propto S(q)$) of the main mode (eq 4) at $q = q^*$ shown in Figure 10 increases with c above

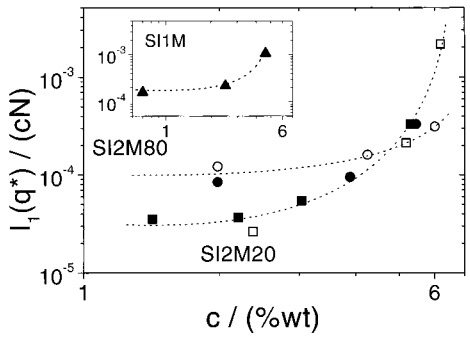

Figure 10. Reduced intensity $I_1(q)/cN$ at $q = 0.034$ nm^{-1} associated with the main chain relaxation in the three SI's. The symbols used denote the same samples as in Figure 8.

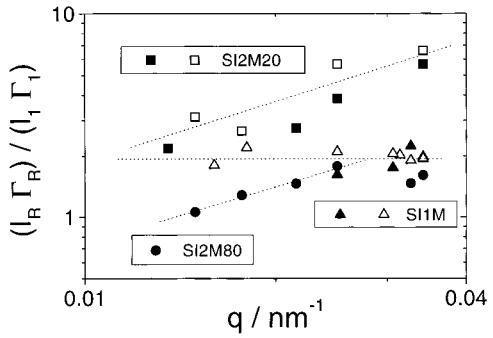

Figure 11. Wave vector dependence of the ratio $(\Gamma_R/\Gamma_1)/(I_1(q)/I_R(q))$ for the three samples in the homogeneous state. Triangles are for the ratio of the fourth symmetric SI1M sample (ref 5).

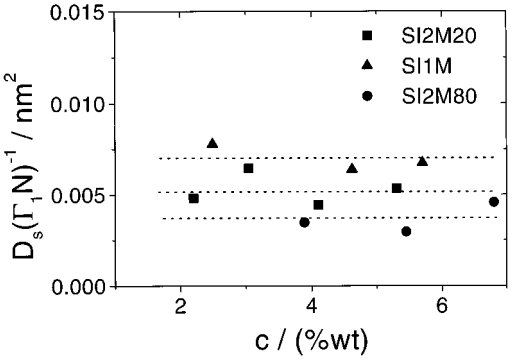

Figure 12. Dynamic quantity $D_s/(\Gamma_1 N)$ for the three SI samples at different concentrations.

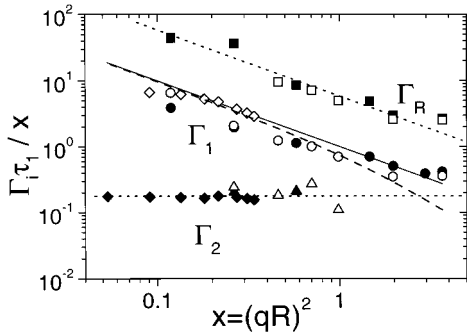

Figure 13. Reduced rates $\Gamma_i\tau_1/x$, respectively, for the polydispersity (Γ_2), collective chain relaxation (Γ_1), and Rouse-like chain motion (Γ_R) in low molecular weight SI (172K) (◆, ●) and the high molecular weight SI2M20 (△, Γ_2; D, Γ_1; □, Γ_R; solid symbols are for SI2M20*). The solid line shows the prediction $g(1,x)/x$ of eq 1 whereas the dotted lines are to guide the eye.

about 2% and 3%, respectively, for SI2M20 ($c_{ODT} = 0.074$ g/cm^3) and SI2M80 ($c_{ODT} = 0.1$ g/cm^3) signalizing the importance of ψ_q^*. For example, SI2M20 exhibits an order of magnitude stronger I_1/cN at 5.4% than below 2%. In the mean field regime, $S(x^*) = (F(f,x^*) - 2\chi^*N)^{-1}$ where $F(x^*)$ is a function of Debye form factors and $\chi^* = \chi f^{1.59}$ is the renormalized[6b] interaction parameter χ. In contrast to the low q-limit (eq 4), $S(x^*)$ ($\propto I_1/cN$) is much more sensitive to the increase of the diblock concentration. However, the analogous slowing down of $\Gamma_1(q^*)$ anticipated from eq 1, is weaker; $\Gamma_1(q^*)$ is only 3 times slower than its value at low q's. (The thermodynamic slowing down of $\Gamma(q \sim q^*)$ and the q dependence of $S(q^*)$ will be the subject of the study near ϕ_{ODT}).[8] What should be emphasized here, however, is the concentration dependence of the polydispersity contribution (Figure 8) S_2 to the total $S(q)$ that cannot be considered to be constant even in the range $3 < \chi^*N < 12$. Note that at ϕ_{ODT}, χ^*N assumes a value of about 30 for the asymmetric SI's while at the phase boundary, if they were blends, the computed $\chi^*N \simeq 11$ and 16 respectively for SI2M20 and SI2M80.

From the two intermediate processes (Figures 3 and 4), the faster mode[9] can be envisaged as curvilinear Rouse-like motions of the entangled chains.[7] This motional mechanism leads[5] to

$$S_R(x,t) = (N_e/6\pi^2)\sum_1 J_1(x)\,\exp[-\Gamma_R{}^2 t] \qquad (5)$$

for the contribution to the intermediate scattering function $S_R(q,t)$ due to one-dimensional Rouse-like motions ($l = 1, 2, ...$). For low x (<1), the main contribution to the $S_R(x)$ arises from the main model $l = 1$ since the intensity factor $I_1 \simeq x/L^2$ and hence the intensity $I_R = (\phi/6\pi^2)N_e(\phi)x$. These tube length fluctuations due to the main Rouse mode occur with a rate

$$\Gamma_R \simeq (3\pi^2/\tau_0)\phi^{-(3\nu-2)/(3\nu-1)}N^{-2} \propto \phi^{-0.3} \qquad (6)$$

displaying clearly weaker concentration dependence than experimentally found (Figure 7). Since both I_R and I_1 scale with x (at low x's), the ratio $I_1/I_R \sim 24/\pi^2 N/N_e(\phi)$ should be insensitive to q variation but N-dependent like the ratio of the rates $\Gamma_R/\Gamma_1 \simeq 3N/N_e(\phi)$. Hence, the quantity $I_R(q)\Gamma_R/(I_1(q)\Gamma_1)$ is predicted to be a constant ($\simeq 3\pi^2/24 = 1.2$). Figure 11 shows this ratio for the three samples using the data of Figures 5 and 6 and ref 5 for a fourth SI1M. It is worth mentioning that while the bulk of the data scatter around 2, the two asymmetric SI2M20 and SI2M80 moieties indicate some clear q dependence. In particular. the enhanced ratio for SI2M20 at high q's relates to the unexpected high I_R (see Figure 5).

To compare the diffusion and chain conformational dynamics among the three samples with different f_s and N and concentration in the examined concentration range far from ODT, we consider the ratio[10] $D/(\Gamma_1 N)$ that virtually amounts to the friction and molecular weight differences. Writing[6] $D \simeq R^2/\tau_1$ with $R^2 = (b^2/6)N$ (b is the statistical segment length), the ratio $D/(\Gamma_1 N) = b^2/3\pi^2$ (for both Rouse and reptation) should be insensitive to concentration variation and yields $b = 3-5$ Å. In fact, this quantity plotted vs c in Figure 12 is virtually c independent but reveals a dependence on block composition which in principle can be attributed to a composition-dependent[11] b and some residual molecular weight dependence not fully accounted for by this ratio.

A reduced relaxation map of the different characteristic time scales of the $\psi_{\mathbf{q}}(t)$ at different q's can be obtained by combining the reduced rates $\Gamma_i\tau_1/x$ of the present high molecular weight SI with low molecular weight SI covering a wide range of reduced length scales x. Such a plot[12] is displayed in Figure 13 for two concentrations of SI2M20 (2 and 4%) and SI ($M_w = 172$ k, $f_s = 0.4$, and $c = 19$ wt %) using exclusively experimental data (PCS and rheology for τ_1). These reduced dynamic quantities should be insensitive to temperature and concentration variations far from ODT as mobility and M_w, effects are minimized. The random phase approximation prediction $\Gamma_1 \propto x^{-1}$ (for monodisperse Rouse diblocks) plotted as solid line captures better the experimental Γ_1 than the $g(1,x)/x$ function.[1c]

IV. Concluding Remarks

Far from the order-to-disorder transition in the disordered state, the utilization of the present high molecular weight diblocks (BC) has elucidated the dynamic contributions to the intermediate scattering function $S(q,t)$. It is now established, that $S(q,t)$ is controlled by three relaxation mechanisms above the estimated crossover volume fraction ϕ_e: two chain conformational motions assigned to reptation-like, Rouse-like backbone motions and one center of mass chain diffusion; the latter is light-scattering inactive for compositionally monodisperse diblocks. It is recognized, however, that a full theoretical account of the observed chain motions of these marginally entangled systems is still missing.

All three rates Γ_i can be represented by a reduced $\Gamma_i\tau_1/x$ vs x plot (Figure 13) where τ_1 is the chain relaxation obtained independently by shear rheometry and $x = (qR)^2$ is the reduced magnification. This experimental time−space plot characterizes the dynamic response of homogeneous BC's.

The effect of the composition heterogeneities[13] in real BC's cannot be considered as a constant addition to the $S(q)$ of monodisperse BC's even far from ODT as revealed by the present decomposition of the dynamic components of the total $S(q)$ usually measured by small-angle X-ray (or neutron) scattering.[14]

Acknowledgment. We are grateful to A. N. Semenov for enlightening discussions and A. Larsen for technical assistance. This research was partially supported by the EU under Grant FMRX-CT97-0112.

References and Notes

(1) Akcasu, A. Z.; Benmouda, M.; Benoit, H. *Polymer* **1986**, *27*, 1935. Erukimovish, I. Ya.; Semenov, A. N. *Zh. Eksp. Fiz.* **1986**, *63*, 259 [*Sov. Phys. JETP* **1986**, *28*, 149]. Fredrickson, G. H. *J. Chem. Phys.* **1986**, *85*, 5306.

(2) Anastasiadis, S. H.; Fytas, G.; Vogt, S.; Fischer, E. W. *Phys. Rev. Lett.* **1993**, *70*, 2415. Fredrickson, G. H.; Bates, F. S. *Annu. Rev. Phys. Chem.* **1996**, *26*, 501.

(3) Jian, T.; Anastasiadis, S. H.; Semenov, A. N.; Fytas, G.; Adachi, K.; Kotaka, T. *Macromolecules* **1994**, *27*, 4762. Pan, C.; Mauer, W.; Lin, Z.; Lodge, T. P.; Stepanek, P.; von Meerwall, E. D.; Watanabe, H. *Macromolecules* 1994, *27*, 4762. Jian, T.; Anastasiadis, S. H.; Fytas, G.; Fleischer, F.; Vilesov, A. D. *Macromolecules* 1995, *28*, 2439. Molina, L. A.; Freire J. *J. Chem. Phys.* **1998**, *109*, 2904.

(4) Chrissopoulou, K.; Rittig, F.; Fytas, G. In *Molecular Interactions and Time-Space Organization in Macromolecular Systems;* Morishima, Y., Norishine, T., Tashiro, K., Eds.; Springer-Verlag: Berlin, 1999.

(5) Semenov, A. N.; Anastasiadis, S. H.; Boudenne, N.; Fytas, G.; Xenidou, M.; Hadjichristidis, N. *Macromolecules* **1997**, *30*, 6280.

(6) Leibler, L. *Macromolecules* **1980**, *13*, 1602. Fredrickson, G. H.; Leibler, L. *Macromolecules* **1989**, 22, 1238.

(7) de Gennes, P. G. *Scaling concepts in Polymer Physics*; Cornell University Press: Ithaca, NY, 1979. Doi, M.; Edwards, S. F. *The Theory of Polymer Dynamics*; Oxford Science Publishers: 1986.

(8) Chrissopoulou, K.; et al. To be published.

(9) This process cannot be the first higher order reptation mode ($k = 1$ in eq 4) with $O(100)$ having less intensity than the main ($k = 0$) mode.

(10) Schweizer, K. S.; Szamel, G. *Macromolecules* **1995**, *28*, 7543.

(11) Binder, K. *J. Chem. Phys.* **1983**, *79*, 6387.

(12) Akcasu, A. Z. In D*ynamic Light Scattering: The Technique and Some Applications*; Brown, W., Ed.; Oxford: New York: 1993.

(13) Burger, C.; Ruland, W.; Semenov, A. N. *Macromolecules* **1990**, *23*, 3339.

(14) Rosedale, J. H.; Bates, F. S.; Almdal, K.; Mortensen, K.; Wignall, G. P. *Macromolecules* **1995**, *28*, 1429. Sakamoto, N.; Hashimoto, T.; Han, C. D.; Kim, D.; Veidya, N. Y. *Macromolecules* **1997**, *30*, 5321.

MA991213F